Computers and Geosciences 112 (2018) 83–100

Contents lists available at ScienceDirect

Computers and Geosciences

journal homepage: www.elsevier.com/locate/cageo

Research paper

Impact of earthquake source complexity and land elevation data resolution on tsunami hazard assessment and fatality estimation

Ario Muhammad [a,b,*], Katsuichiro Goda [a]

[a] Department of Civil Engineering, University of Bristol, Bristol BS8 1TR, UK
[b] Department of Civil Engineering, Narotama University, Surabaya, Indonesia

ARTICLE INFO

Keywords:
DEM resolution
Earthquake source complexity
Tsunami hazard
Tsunami fatality
Big data

ABSTRACT

This study investigates the impact of model complexity in source characterization and digital elevation model (DEM) resolution on the accuracy of tsunami hazard assessment and fatality estimation through a case study in Padang, Indonesia. Two types of earthquake source models, i.e. complex and uniform slip models, are adopted by considering three resolutions of DEMs, i.e. 150 m, 50 m, and 10 m. For each of the three grid resolutions, 300 complex source models are generated using new statistical prediction models of earthquake source parameters developed from extensive finite-fault models of past subduction earthquakes, whilst 100 uniform slip models are constructed with variable fault geometry without slip heterogeneity. The results highlight that significant changes to tsunami hazard and fatality estimates are observed with regard to earthquake source complexity and grid resolution. Coarse resolution (i.e. 150 m) leads to inaccurate tsunami hazard prediction and fatality estimation, whilst 50-m and 10-m resolutions produce similar results. However, velocity and momentum flux are sensitive to the grid resolution and hence, at least 10-m grid resolution needs to be implemented when considering flow-based parameters for tsunami hazard and risk assessments. In addition, the results indicate that the tsunami hazard parameters and fatality number are more sensitive to the complexity of earthquake source characterization than the grid resolution. Thus, the uniform models are not recommended for probabilistic tsunami hazard and risk assessments. Finally, the findings confirm that uncertainties of tsunami hazard level and fatality in terms of depth, velocity and momentum flux can be captured and visualized through the complex source modeling approach. From tsunami risk management perspectives, this indeed creates big data, which are useful for making effective and robust decisions.

1. Introduction

Recent advances in geosciences have drastically enhanced the accuracy of numerical simulations of complex natural phenomena, such as earthquake rupture processes and consequent earthquake motions and tsunamis (Wang et al., 2015; Ismail-Zadeh et al., 2017). In tsunami sciences, the improvements lead to sophistication in earthquake source modeling and availability of high-resolution bathymetry and digital elevation models (DEMs), which enhance the quality of tsunami simulations (Ridente et al., 2014; Ramírez-Juidías et al., 2017). Consequently, these progresses in turn have promoted more rigorous treatment and visualization of uncertainties associated with tsunami disaster risk management.

In general, tsunami risk can be evaluated by convoluting exposure, tsunami hazard, and vulnerability (Chorafas, 2004; Attary et al., 2017). Among the three key elements of tsunami risk, tsunami hazard assessment can be carried out in three stages: tsunami source modeling, propagation, and inundation (Srisutam and Wagner, 2010; Sleeter et al., 2017). Typically, the tsunami hazard assessment results are significantly affected by the source and inundation modeling because those are subjected to large uncertainties (Mueller et al., 2015; Schäfer and Wenzel, 2017). On the other hand, a well-established methodology, e.g. linear/non-linear shallow water equations, has been verified and widely used for tsunami propagation modeling (King, 2015; Park and Cox, 2016; Feng et al., 2017). Given accurate offshore bathymetry data, e.g. GEBCO and SRTM15-plus, propagation components involve relatively less uncertainties and can be regarded as solved problems (Feng et al., 2017).

Nowadays, so-called source inversion analyses have been conducted using various types of data from teleseismic, strong motion, GPS, and tide gauge stations. One example of such developments can be seen by

* Corresponding author. Department of Civil Engineering, University of Bristol, Bristol BS8 1TR, UK.
E-mail address: ario.muhammad@bristol.ac.uk (A. Muhammad).

https://doi.org/10.1016/j.cageo.2017.12.009
Received 29 May 2017; Received in revised form 26 September 2017; Accepted 15 December 2017
Available online 16 December 2017

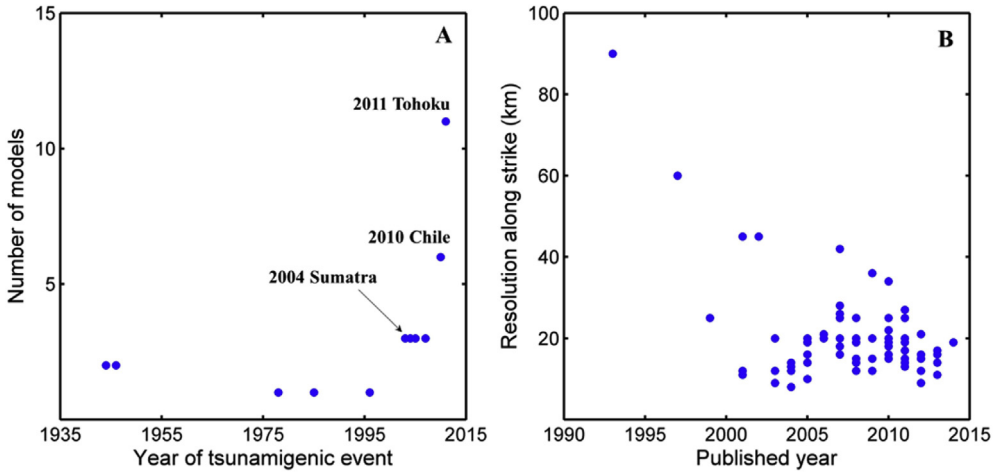

Fig. 1. Trend of finite-fault models in the SRCMOD database in terms of published year (a) number of the models and (b) resolution of the models.

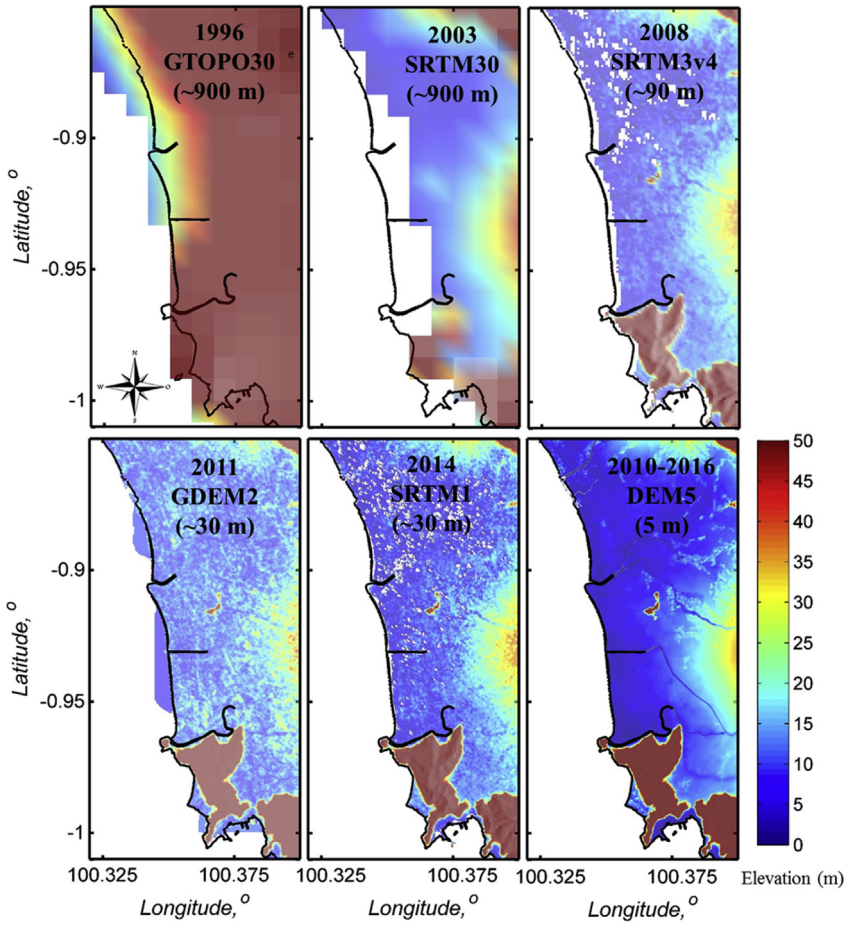

Fig. 2. Comparison of global DEMs in Padang, Indonesia.

examining the fast-growing size of earthquake source model databases, such as SRCMOD (Mai and Thingbaijam, 2014; http://equake-rc.info/SRCMOD/). The SRCMOD database is an online database of finite-fault rupture models of past earthquakes around the world. As of June 2017, 334 finite-fault models from 169 earthquakes are available. About 109 out of 334 models are for tsunamigenic earthquakes generated from subduction zones and its number, especially for large tsunamigenic events, is increasing steadily (Fig. 1A). One notable trend of the SRCMOD database is the change of the resolution of source model descriptions over time (Fig. 1B); more models have been developed by capturing finer details of the rupture processes. Moreover, gathered finite-fault models can be used to characterize source parameters (geometry and slip features) for subduction earthquakes and therefore can be adopted to develop new statistical prediction models of the parameters for future

Table 1
Scaling relationships of the earthquake source parameters (Goda et al., 2016). The prediction error terms of the scaling relationships are represented by epsilons, which are the standard normal variables (i.e. zero mean and unit standard deviation).

Parameter	Prediction models
W	$\log_{10}W = -0.4877 + 0.3125M_w + 0.1464\varepsilon_W$
L	$\log_{10}L = -1.5021 + 0.4669M_w + 0.1717\varepsilon_L$
D_a	$\log_{10}D_a = -5.7933 + 0.7420M_w + 0.2502\varepsilon_{Da}$
D_m	$\log_{10}D_m = -4.5761 + 0.6681M_w + 0.2249\varepsilon_{Dm}$
A_z	$\log_{10}A_z = -1.0644 + 0.3093M_w + 0.1592\varepsilon_{Az}$
A_x	$\log_{10}A_x = -1.9844 + 0.4520M_w + 0.2204\varepsilon_{Ax}$
Box-Cox power	A normal variable with mean equal to 0.312 and standard deviation equal to 0.278
Hurst number	A value of 0.99 with probability of 0.43 and a normal variable with mean equal to 0.714 and standard deviation equal to 0.172 with probability of 0.57

Table 2
Linear correlation coefficients of regression residuals of the scaling relationships for the six earthquake source parameters. Note that the Box-Cox parameter and the Hurst number are considered to be independent.

Variables	ε_W	ε_L	ε_{Da}	ε_{Dm}	ε_{Az}	ε_{Ax}
ε_W	1	0.139	−0.68	−0.545	0.826	0.035
ε_L	0.139	1	−0.595	−0.516	0.249	0.734
ε_{Da}	−0.68	−0.595	1	0.835	−0.62	−0.374
ε_{Dm}	−0.545	−0.516	0.835	1	−0.564	−0.337
ε_{Az}	0.826	0.249	−0.62	−0.564	1	0.288
ε_{Ax}	0.035	0.734	−0.374	−0.337	0.288	1

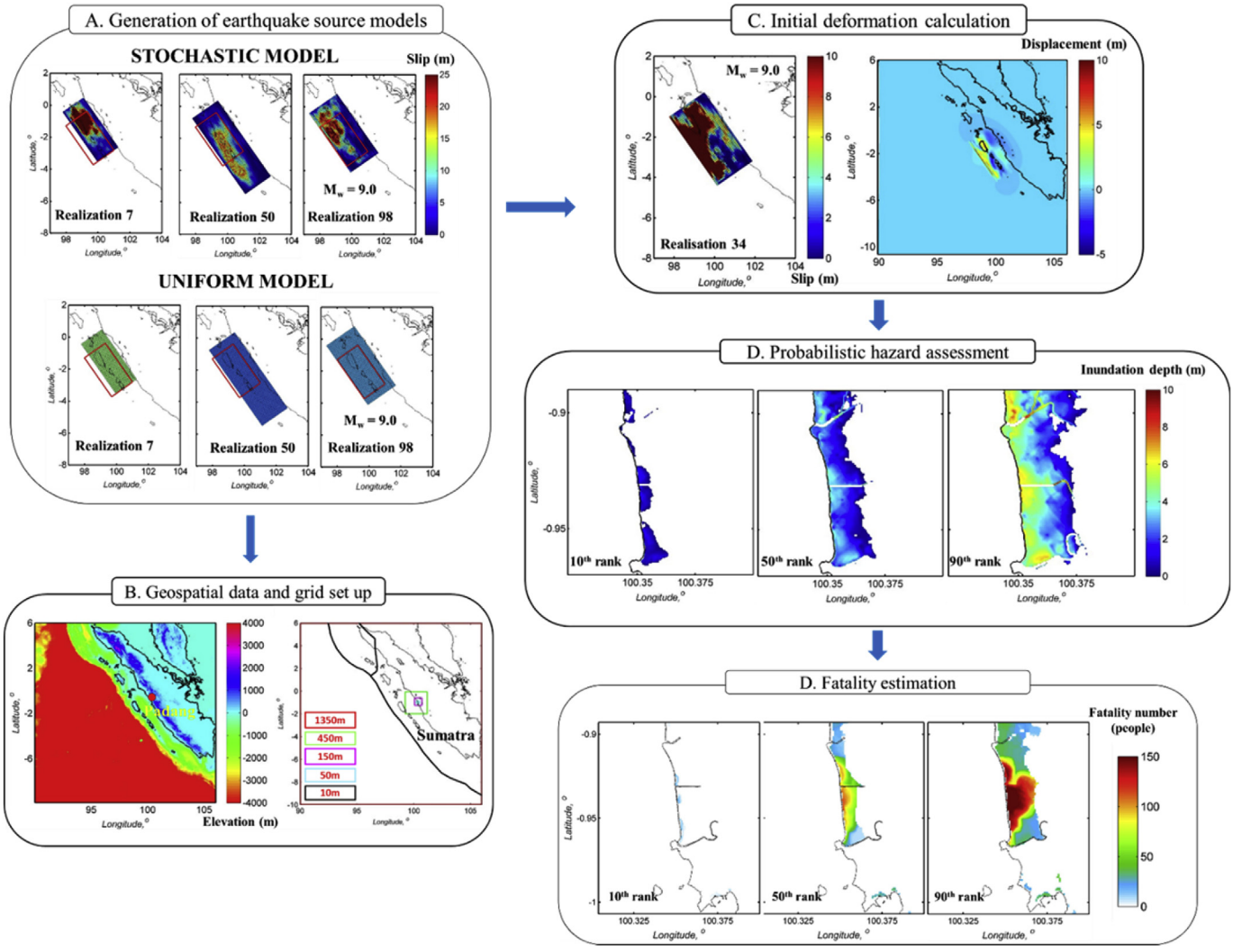

Fig. 3. Procedure of tsunami hazard assessment and fatality estimation.

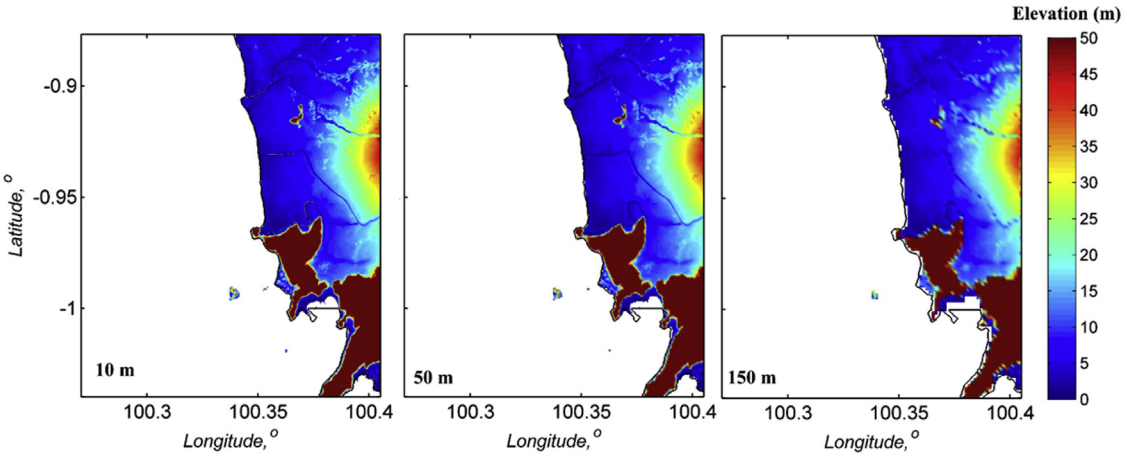

Fig. 4. DEM profiles in Padang.

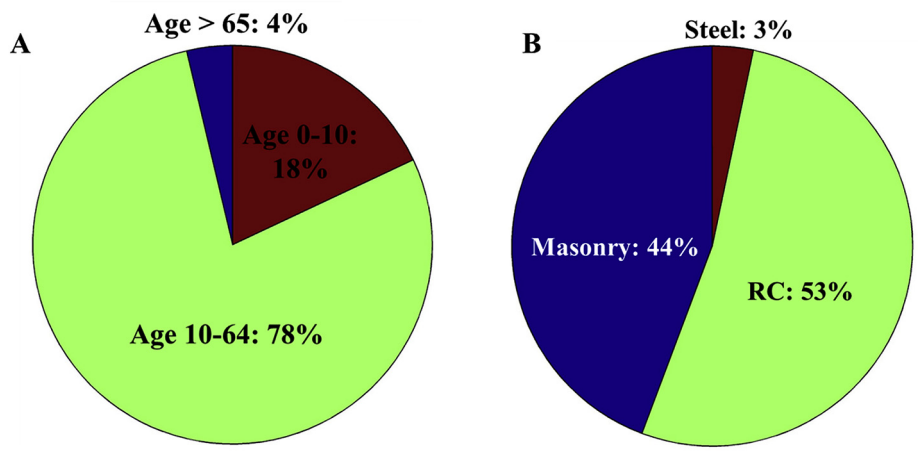

Fig. 5. (A) Age distribution of Padang population. (B). Building type percentage in Padang.

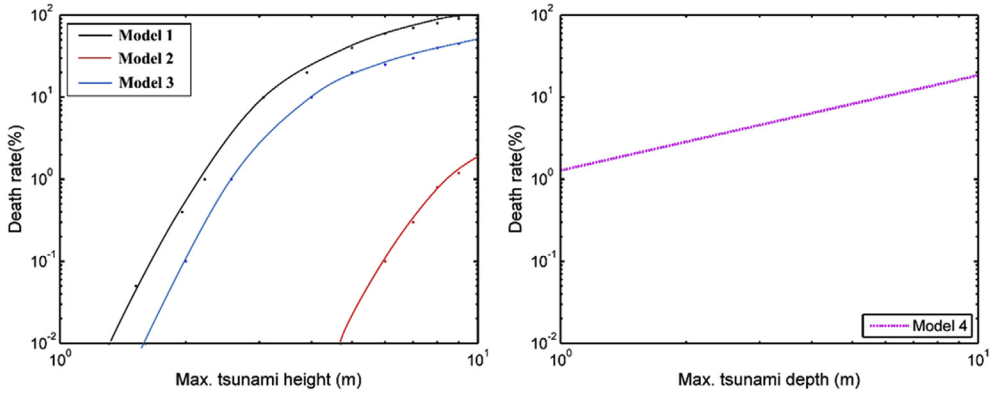

Fig. 6. Fatality models adopted in this study.

tsunamigenic scenarios (Goda et al., 2016). These new statistical prediction models may be used to generate the heterogenous/complex slip models and hence, can be used to rigorously study the effects of earthquake source complexity on the tsunami hazard assessment and fatality estimation.

For inundation modeling, a major source of uncertainty can be attributed to land DEM data in coastal areas (Griffin et al., 2015; Farahani et al., 2017), which have been significantly improved in the last two decades. The spatial resolution of global elevation data has been improved from ~900 m (GTOPO30) in 1990s to ~30 m (SRTM1) in 2014 (see Fig. 2). Moreover, data with resolutions up to 10 m or less (e.g. 5 m in Padang areas) are available at the regional scale using the advanced satellite and aerial photography. Such improvements lead to accurate evaluations of tsunami hazard metrics, such as depth and flow velocity

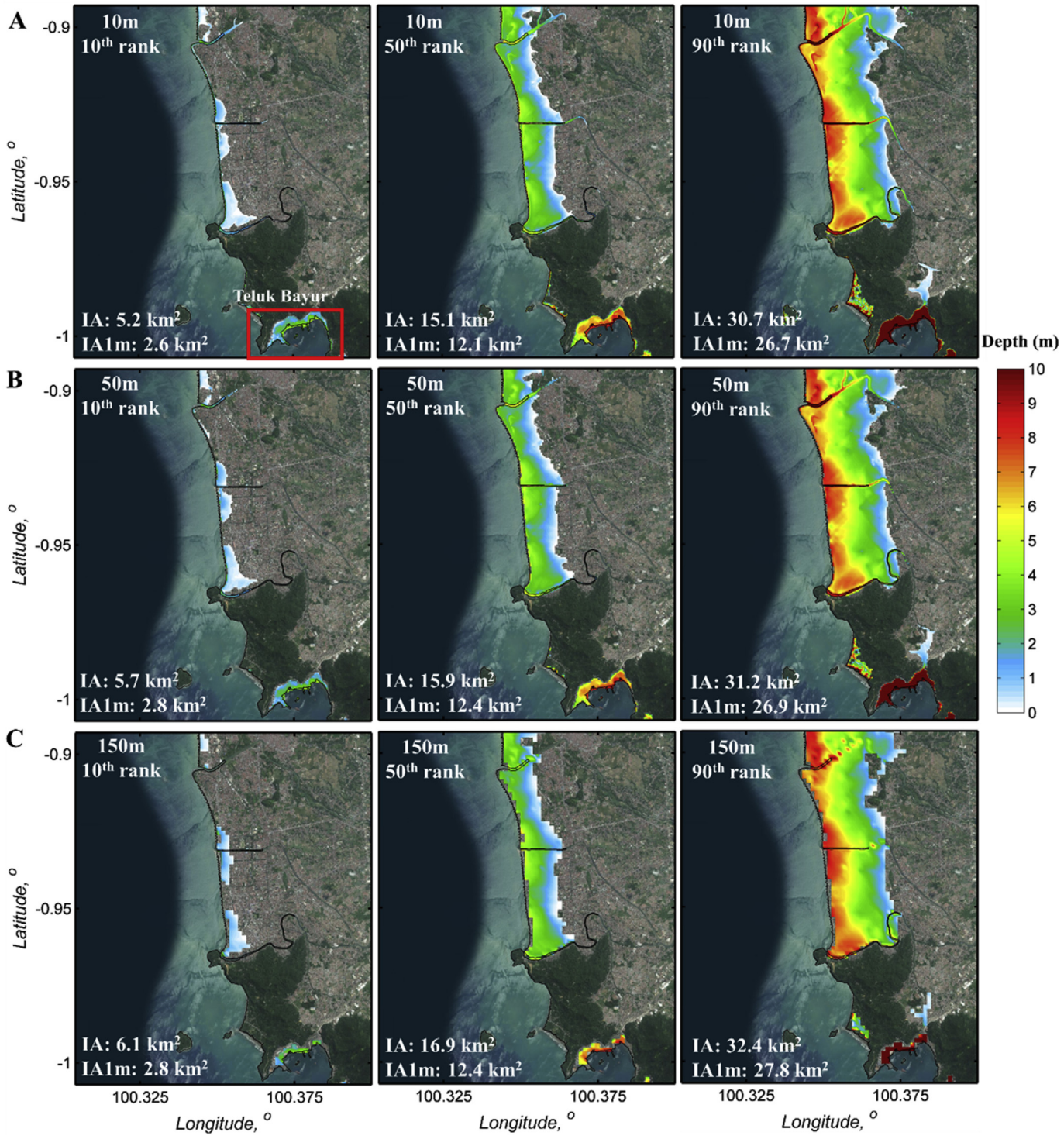

Fig. 7. Tsunami depth in Padang from stochastic model. (A) 10-m resolution. (B) 50-m resolution. (C). 150 m-resolution. (IA = Inundation area; IA1m = Inundation area above 1 m depth).

(De Risi et al., 2017).

Building upon the above findings, this study aims at evaluating the impact of source characterization complexity and DEM resolution on the accuracy of tsunami hazard assessment and fatality estimation. This study is focused upon Padang, West of Sumatra, Indonesia which is one of the most tsunami-prone areas around the world due to future tsunamigenic events from the Mentawai segment of the Sunda subduction zone (Diana et al., 2014; Alvina et al., 2015; Muhammad et al., 2016, 2017). Two future scenarios (M_w 9.0) of earthquake sources in the Mentawai-Sunda zone are generated by considering (1) uniform-slip source models with variable fault geometry and mean slip and (2) complex source models with heterogeneous slip distribution. 100 uniform-slip source models are used, whilst 300 stochastic source models are generated using new statistical prediction models of source parameters that are based on finite-fault models of the past subduction earthquakes (Muhammad et al., 2016). Moreover, for inundation modeling, three elevation resolutions, i.e. 150 m, 50 m and 10 m, are considered and hence, a total of 1200 scenarios are developed in this study. It is

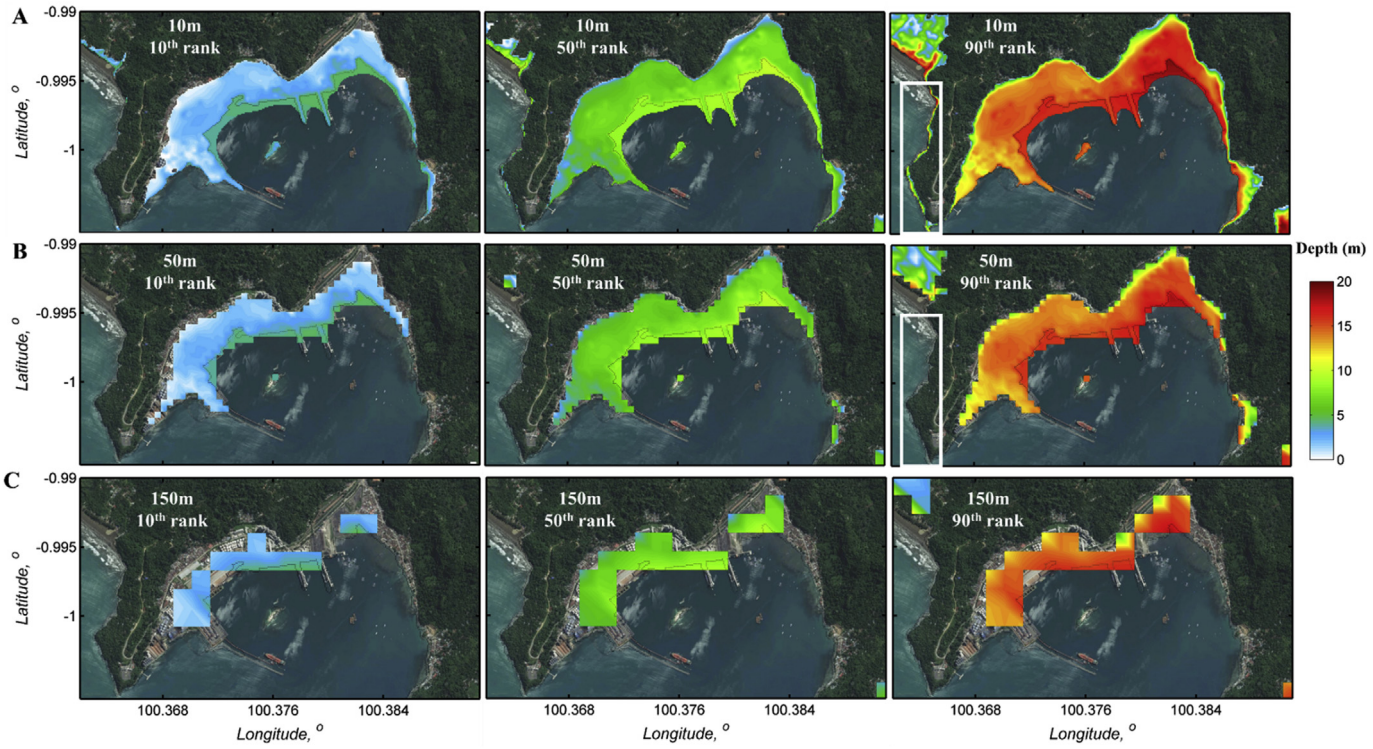

Fig. 8. Tsunami depth in Teluk Bayur from stochastic model. (A) 10-m resolution. (B) 50-m resolution. (C). 150 m-resolution.

noteworthy that stochastic source models are particularly useful for capturing the uncertainties associated with earthquake ruptures, and that use of stochastic sources in tsunami hazard and risk assessments allows a new way of summarizing the hazard and risk analysis results. In other words, new probabilistic approaches create big data for more robust and effective tsunami risk management. In this study, a tsunami hazard is the main focus without accounting for other earthquake impacts (e.g. shaking damage and ground failures) and hence, the fatality estimation also excludes the earthquake effects. Therefore, the results reported in this paper constitute the lower bound estimate of fatalities due to the mega-thrust subduction earthquakes. Potential earthquake impacts have been discussed in Muhammad et al. (2017). The scope of this study was limited partly due to unavailability of extensive building information data for Padang areas (Schlurmann et al., 2010; Muhari et al., 2010, 2011), which is necessary for evaluating both earthquake and tsunami losses quantitatively.

2. Methodology

2.1. Modeling of tsunami sources

Two critical factors to determine earthquake sources for the future tsunamigenic events are earthquake location and source parameters (e.g. fault geometry and slip distribution). In general, the locations of earthquake source scenarios are defined based on the fault rupture areas of the past seismic events in a region of interest (Martínez-Álvarez et al., 2015; Abril and Periáñez, 2017). On the other hand, the earthquake source parameters are determined using empirical scaling relationships that are typically generated based on historical events (e.g. Wells and Coppersmith, 1994; Somerville et al., 1999; Mai and Beroza, 2002; Strasser et al., 2010; Murotani et al., 2013; Thingbaijam et al., 2017). The empirical relationships between moment magnitude (M_w) and other earthquake source parameters, e.g. rupture length, rupture width, rupture area, and slip statistics, have been developed extensively since 1950s (e.g. Tocher, 1958; Iida, 1959). Among the existing global scaling laws, the scaling laws developed by Goda et al. (2016) may be considered as one of the most comprehensive and reliable scaling laws to determine earthquake source parameters of future tsunamigenic events from the Mentawai segment of the Sunda subduction areas because of the following reasons. First, it was developed using extensive finite-fault models of the past subduction earthquakes around the world (i.e. 226 models). Second, it incorporated the uncertainty and dependency of essential earthquake source parameters using multivariate probabilistic models, i.e. fault geometry parameters (the fault width, W, and fault length, L), slip statistics parameters (mean slip, D_a, maximum slip, D_m, and Box-Cox number, λ and spatial heterogeneity slip parameters (correlation lengths along strike, A_x, and dip, A_z, directions and Hurst number, H), and third, It was successfully modelled the future tsunamigenic earthquake source scenarios generated from the Mentawai-Sunda zone, Indonesia by considering the regional seismological characteristic of the Sunda subduction zone (see Muhammad et al., 2016 and Muhammad et al., 2017).

Table 1 lists the scaling relationships for W, L, D_a, D_m, A_z, and A_x, respectively, by Goda et al. (2016). In the equations, epsilon terms represent the prediction errors of the equations and thus the relationships are probabilistic. Furthermore, their correlation coefficients are given in Table 2. Stochastic slip models can be simulated by taking into account all uncertainty and dependency of the earthquake source parameters presented in Table 2 (Goda et al., 2016; Muhammad et al., 2016; Mori et al., 2017). A spectral synthesis method is adopted to model the stochastic earthquake slip by characterizing earthquake slip distribution with wavenumber spectra (see Mai and Beroza, 2002; Goda et al., 2014 for details). Subsequently, a total of 300 stochastic models and 100 uniform models of future tsunamigenic earthquakes in the Mentawai-Sunda zone are generated using the new scaling relationships. The generated stochastic source models have heterogeneous spatial slips over the fault plane simulated through stochastic earthquake slip synthesis (see the top panel of Fig. 3A). On the other hand, the uniform models have variations of fault geometry and mean slip with a constant slip value over the fault plane taken from the generated mean slip (see the bottom panel of Fig. 3A). The numbers of source models for complex and

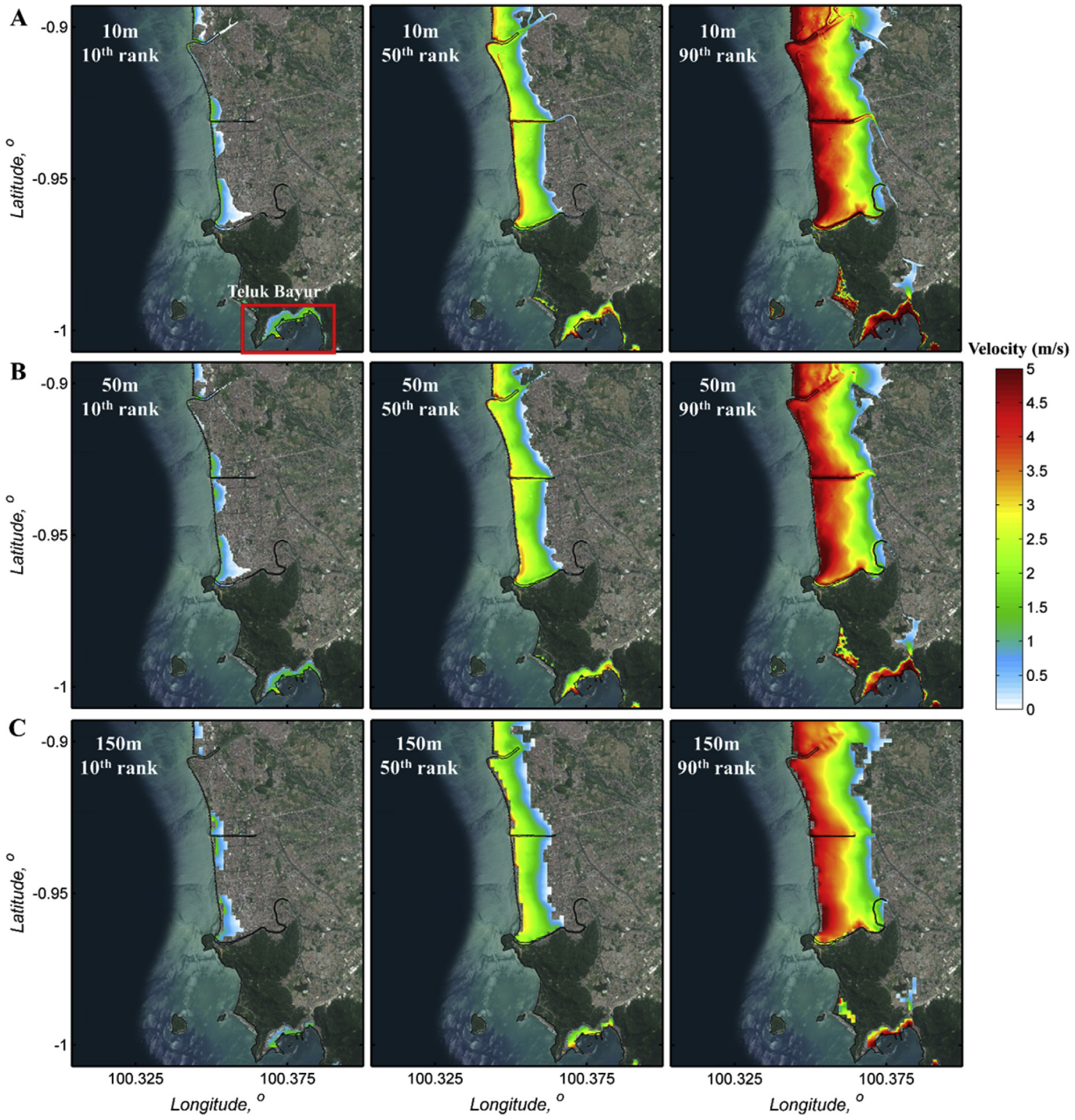

Fig. 9. Tsunami velocity in Padang from stochastic models. (A) 10-m resolution. (B) 50-m resolution. (C). 150 m-resolution.

uniform cases, i.e. 300 and 100, respectively, were determined based on the convergence tests of the various tsunami outputs. The convergence tests were carried out by evaluating the stability of tsunami simulation results (i.e. maximum tsunami depth and height) against the number of simulations for each type of earthquake source complexity (see De Risi and Goda, 2016).

2.2. Elevation data for tsunami simulation

In this study, local data of 5 m-DEM (DEM5) and 3 m-bathymetry (Bathy3m) are used to produce elevation data for tsunami simulation. DEM5 was generated through the German Indonesian Tsunami Early Warning System for the Indian Ocean (GITEWS) project. The DEM5 was developed by combining extensive remote sensing data including high-resolution satellite imagery from the IKONOS and GPS measurements. On the other hand, to obtain the Bathy3m data, ship sounding surveys were carried out near shore Padang with depth ranges from 3 m to 50 m. An accuracy assessment of DEM5 and Bathy3m shows that the vertical errors of these elevation data are about 0.5 m. The vertical error for land elevation in DEM5 was calculated from the comparison with the

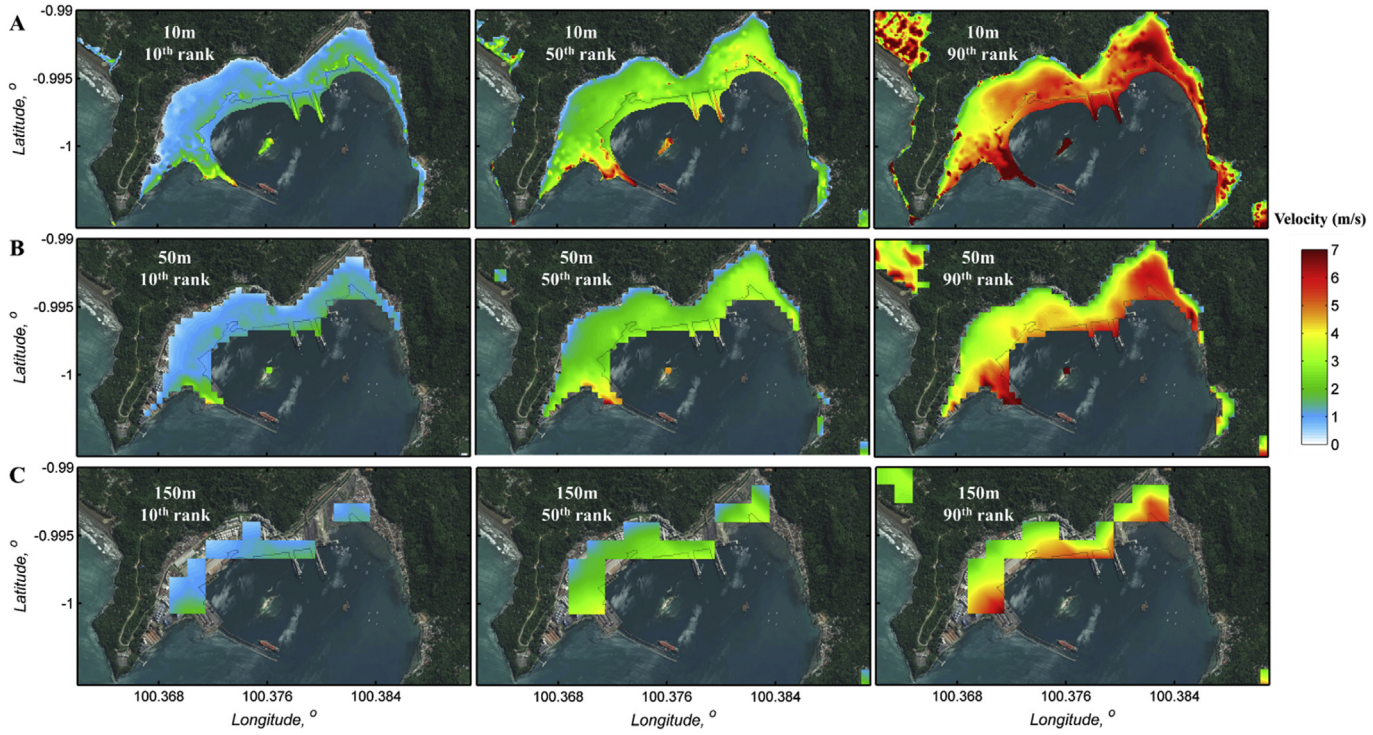

Fig. 10. Tsunami velocity in Teluk Bayur from stochastic source models. (A) 10-m resolution. (B) 50-m resolution. (C). 150 m-resolution.

observed data using GPS measurements. The error of ocean depth in the Bathy3m dataset was estimated based on the accuracy of echo sounder device used for ocean depth measurements, noting that the error of the sounding depth is only ~0.2% (Taubenbock et al., 2009; Schlurmann et al., 2010). Therefore, it is considered as a reliable dataset for tsunami hazard and risk assessments. Moreover, missing land elevation and bathymetry data which are not covered in those datasets are supplemented from GDEM2 (https://asterweb.jpl.nasa.gov/gdem.asp) and GEBCO2014 (http://www.gebco.net/data_and_products/gridded_bathymetry_data/), respectively.

The nested grid systems having five levels (connected with a grid-size ratio of 3) are further developed: 1350 m, 450 m, 150 m, 50 m, and 10 m (see Fig. 3B). Subsequently, to study the effects of elevation data resolution on tsunami hazard assessment and fatality estimation, three finest grid levels of land elevation data, i.e. 150 m, 50 m, and 10 m, are considered. The 150-m grid is used to represent the coarse resolution, whilst 30-m to 50-m is a typical finer resolution for tsunami simulation in a region near Padang (Yue et al., 2014; Griffin et al., 2015). On the other hand, the 10-m grid is taken into account since the other hazard parameters, such as flow velocity and momentum flux, are found to be sensitive to the tsunami simulation resolution even though the computational cost is expensive (De Risi and Goda, 2016). Fig. 4 presents the DEM profiles of three grid resolutions for tsunami simulation. Visually, the DEM appearances for the 10-m and 50-m grid resolutions are similar, whilst it is relatively blur for the 150-m grid.

The initial deformation of sea bed is calculated based on the generated source models by considering both horizontal and vertical displacements of the seafloor using Okada (1985) and Tanioka and Satake (1996) formulae (see Fig. 3C). Tsunami simulation is then carried out by solving non-linear shallow water equation with run up (Goto et al., 1997). In this study, the effect of roughness coefficient on tsunami hazard assessment is not investigated due to lack of detailed information for the coefficient in Padang. The roughness coefficient of 0.025 $m^{-1/3}s$ is used for ocean because the simulated offshore tsunami wave height using this value can be matched well with the observation data from the past events, such as the 2004 Indian Ocean tsunami (Imamura, 2009; Sugawara and Goto, 2012). Moreover, the roughness coefficient for land has relatively small impact when the value is changed from 0.025 $m^{-1/3}s$ to 0.08 $m^{-1/3}s$ (Griffin et al., 2015) and hence, a value of 0.06 $m^{-1/3}s$ is adopted for land because the inundation inland produces from this value agreed well with the observed tsunami inundation depth from the 2004 and the 2011 Tohoku events (Kaiser et al., 2011; Griffin et al., 2015). The fault rupture is assumed to occur instantaneously. Moreover, the duration of the tsunami simulation is set to 2 h and the time step is varied from 0.1 s to 1 s depending on the grid resolution. This set up satisfies the Courant-Friedrichs-Lewys (C.F.L.) criterion for the bathymetry and elevation data of the Mentawai-Sunda region. The Monte Carlo tsunami simulation is finally performed using different initial deformation profiles calculated from the generated uniform and complex source models.

2.3. Tsunami hazard assessment

Results from the Monte Carlo tsunami simulation based on the generated earthquake source models can be used to produce probabilistic tsunami hazard results in a region of interest and further used for risk assessment (see Fig. 3D and E). In this study, three tsunami hazard parameters, i.e. maximum tsunami depth (H_{max}), maximum flow velocity (V_{max}), and momentum flux (M_{F-max}), are considered. Tsunami depth/height and velocity are popular parameters to represent the tsunami hazard level in the affected areas and have been extensively used to assess the tsunami hazard (Charvet et al., 2015; Park and Cox, 2016). On the other hand, momentum flux, calculated as the squared velocity multiplied by inundation depth (see Equation (3)), has been found to represent the tsunami hydrodynamic force on structures and are related to the building damage probability (FEMA, 2012; Park and Cox, 2016; Park et al., 2017). The spatial data of such tsunami force and impact parameters generated from the future tsunamigenic events will enable coastal planners to identify high risk regions and locate new development in safer areas.

The maximum tsunami inundation depth (H_{max}) at each location (x

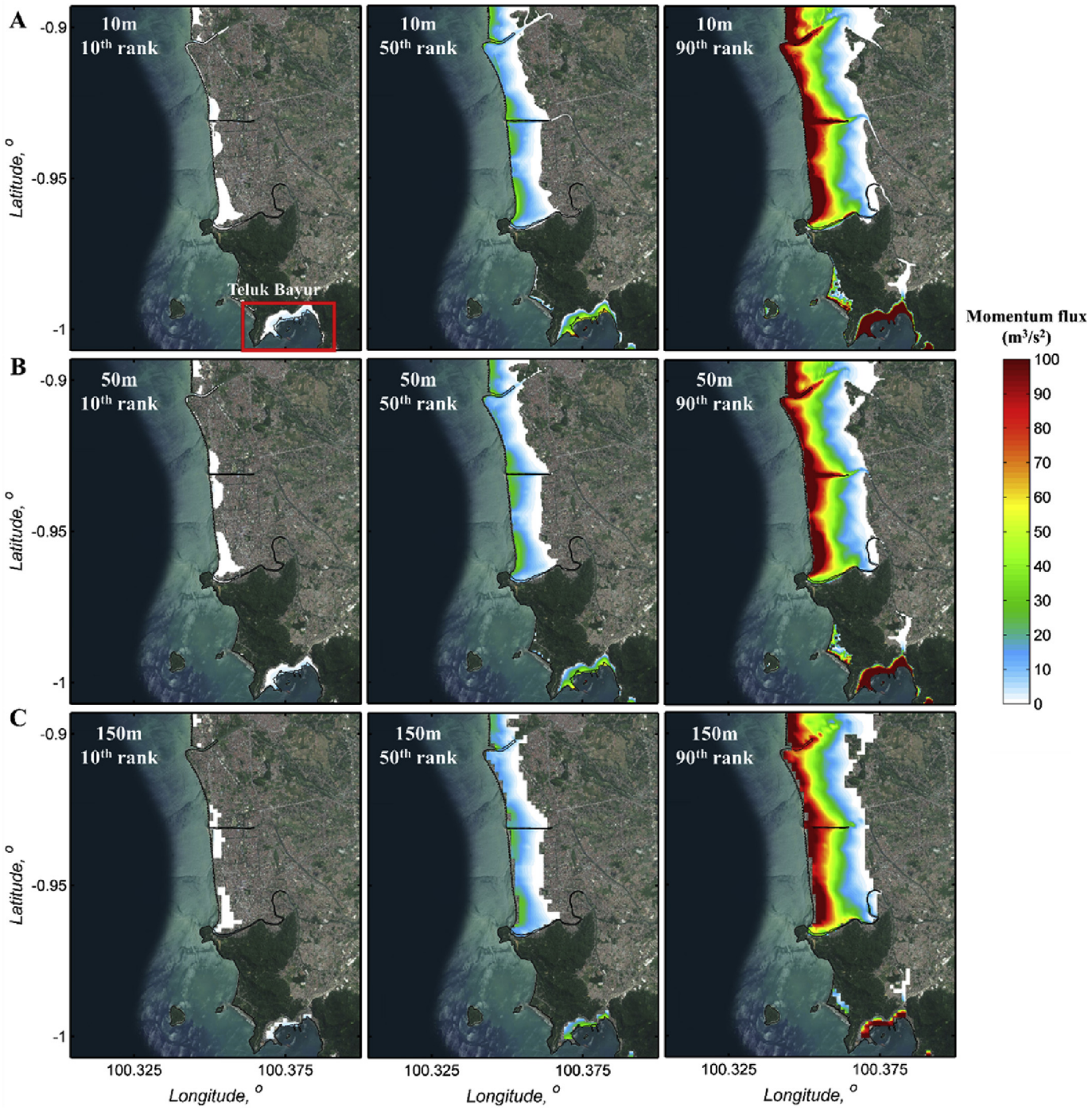

Fig. 11. Momentum flux in Padang from stochastic models. (A) 10-m resolution. (B) 50-m resolution. (C) 150 m-resolution.

and y) is calculated by taking the difference between the maximum tsunami height (η) and the elevation (H_{land}) at a point of interest (Equation (1)).

$$H_{max}(x,y) = [\eta(x,y,t)]_{max} - H_{land}(x,y) \quad (1)$$

The tsunami velocity (V_{max}) at each point (x and y) used in this work is the resultant velocity of the maximum velocity in X and Y directions (u and v, respectively) from each simulation time step, t, calculated using Equation (2).

$$V_{max}(x,y) = \sqrt{[v(x,y,t)]^2_{max} + [u(x,y,t)]^2_{max}} \quad (2)$$

In addition, the maximum momentum flux (M_{F-max}) is calculated by taking the maximum value of multiplication between the tsunami depth and the squared velocity at each point as presented in Equation (3) (FEMA, 2012; Park and Cox, 2016).

$$M_{F-max}(x,y,t) = \left[H(x,y,t) \times V^2(x,y,t)\right]_{max} \quad (3)$$

2.4. Fatality estimation

2.4.1. Demographic features of Padang

Padang is one of the most urbanized areas, having the highest population density in West of Sumatra. A total area of Padang is 695 km^2,

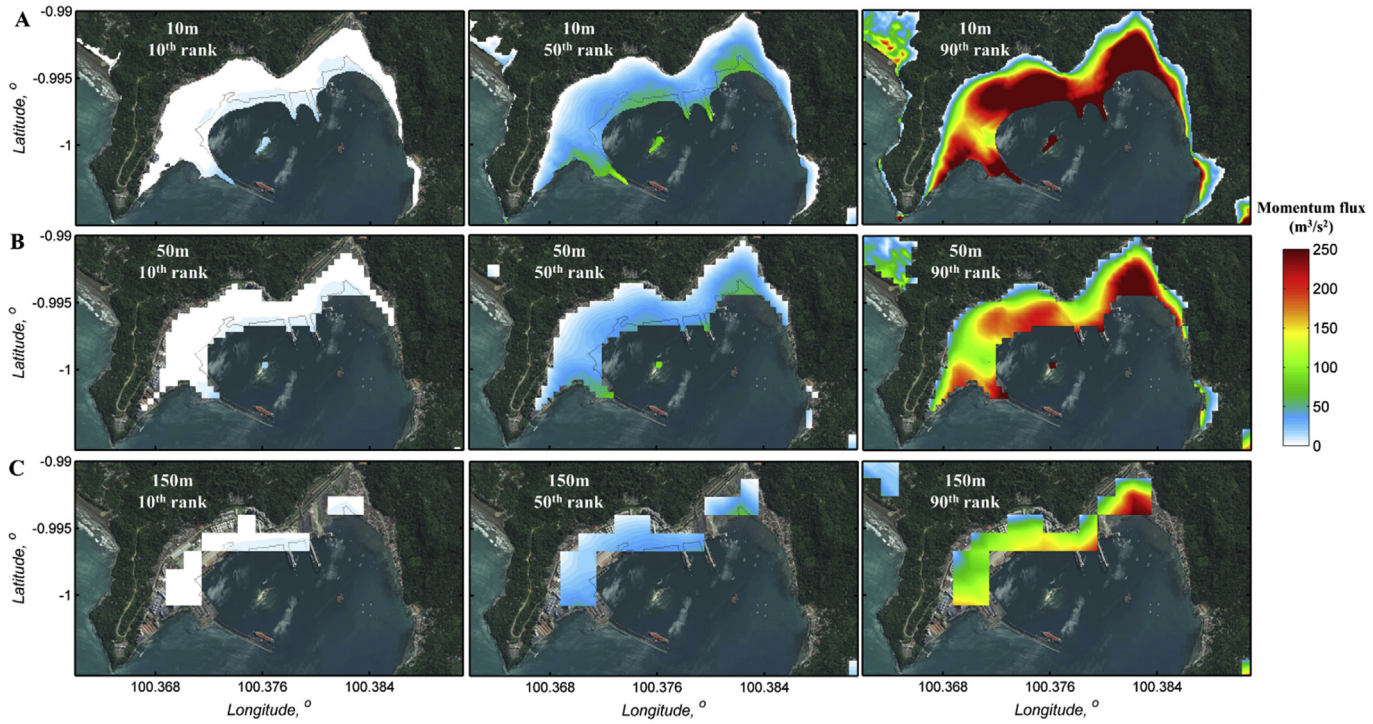

Fig. 12. Momentum flux in Teluk Bayur from stochastic models. (A) 10-m resolution. (B) 50-m resolution. (C). 150 m-resolution.

whilst its total population and population density in 2013 reported by the Indonesian Central Bureau of Statistics (BPS) were 876,678 people and 1349 people/km^2, respectively (BPS, 2013). Most of the population (78%) are in teenage to adult category (10–64 years old) with 50% from this category are in the age of 15–40 years old. On the other hand, the percentage of elderly is relatively small (4%) and that for infants and children is about 17% (see Fig. 5A). Subsequently, the mobility during the evacuation is not critical. In this study, the population data obtained from the WorldPop database are adopted (http://www.worldpop.org.uk/). The WorldPop database includes high-resolution population maps (approximately 100 m by 100 m resolution) of Padang in year 2010, 2015, and 2020. By incorporating various geographical and demographic data, the WorldPop database has been constructed. The population numbers of WorldPop data (2015) in Padang (i.e. South, North, West, and East of Padang) are slightly smaller than the BPS data (2013; i.e. 500,000 people for the WorldPop, whilst it is 510,000 people for the BPS). In this study, the population data in 2015 are used to estimate the fatality due to the future tsunamigenic event. Moreover, building structures in Padang are mainly categorized as unreinforced masonry, confined masonry, and reinforced concrete (RC) frames with masonry fills (see Fig. 5B for details; Wilkinson et al., 2012; Mulyani, 2013).

2.4.2. Fatality estimation

Several models in predicting fatality have been developed using observed tsunami hazard parameters (i.e. tsunami height, depth and building damage) from the past tsunami events, e.g. the 2004 Aceh-Andaman tsunamigenic earthquake and the 2011 Tohoku earthquake (Kawata, 1997; Marchand et al., 2009; Yeh, 2010; Suppasri et al., 2012, 2016). Typically, the death rate (DR) is used to estimate fatality in a region of interest. In order to determine appropriate fatality models for calculating fatality in Padang, three criteria are further adopted. First, the model is developed through extensive tsunami survey data from the historical tsunami events and/or is the most updated fatality model in current literature. Second, the model is developed by assuming only one parameter (i.e. tsunami depth or height) used to calculate the fatality without considering other parameters (e.g. people evacuation and building damage probability). Third, the model has been evaluated or successfully calibrated for the fatality number observed in Banda Aceh, Sumatra due to the 2004 Aceh-Andaman tsunami. The last criterion is because current situations of tsunami mitigation measures in Padang resemble those in Banda Aceh. Therefore, in this study, four fatality models (see Fig. 6) are taken into account: two variations of the models by Kawata (1997), a model by Suppasri et al. (2012), and a model by Suppasri et al. (2016). Model 1 and model 2 were developed by Kawata (1997) with and without considering the existing evacuation plan. Model 3 (Suppasri et al., 2012) revised model 1 to match with observational fatality data in Banda Aceh. The first three models use tsunami height to calculate death rate. In addition, model 4 was generated by Suppasri et al. (2016) considering tsunami height to calculate the death rate.

Total number of fatality (TC) is finally calculated by summing all fatalities occurred in each inundation point (x and y). Assuming tsunami hazard parameter (TP) at x and y represents maximum inundation height, η_{max}, or maximum inundation depth, H_{max}, and death rate, DR, occurred at the expected inundation point, the total fatality is further calculated using Equation (4).

$$TC = \sum [DR(x,y) \times TP(x,y)] \tag{4}$$

3. Results and discussions

3.1. Effect of DEM resolution on tsunami hazard assessment

Tsunami depth, velocity, and momentum flux maps of Padang areas for the three DEM resolutions using stochastic models are shown in Figs. 7, 9 and 11, respectively. For each tsunami hazard parameter map, three probability ranks, i.e. the 10th percentile rank, the 50th percentile rank, and the 90th percentile rank out of 300 source models, are included as summary statistics. In addition, total inundation areas and total inundation areas above 1 m depth are also presented in the maps. The 1-m depth is adopted because at this water level, evacuation may be difficult. Visually, the tsunami depth maps produced from the 10-m and

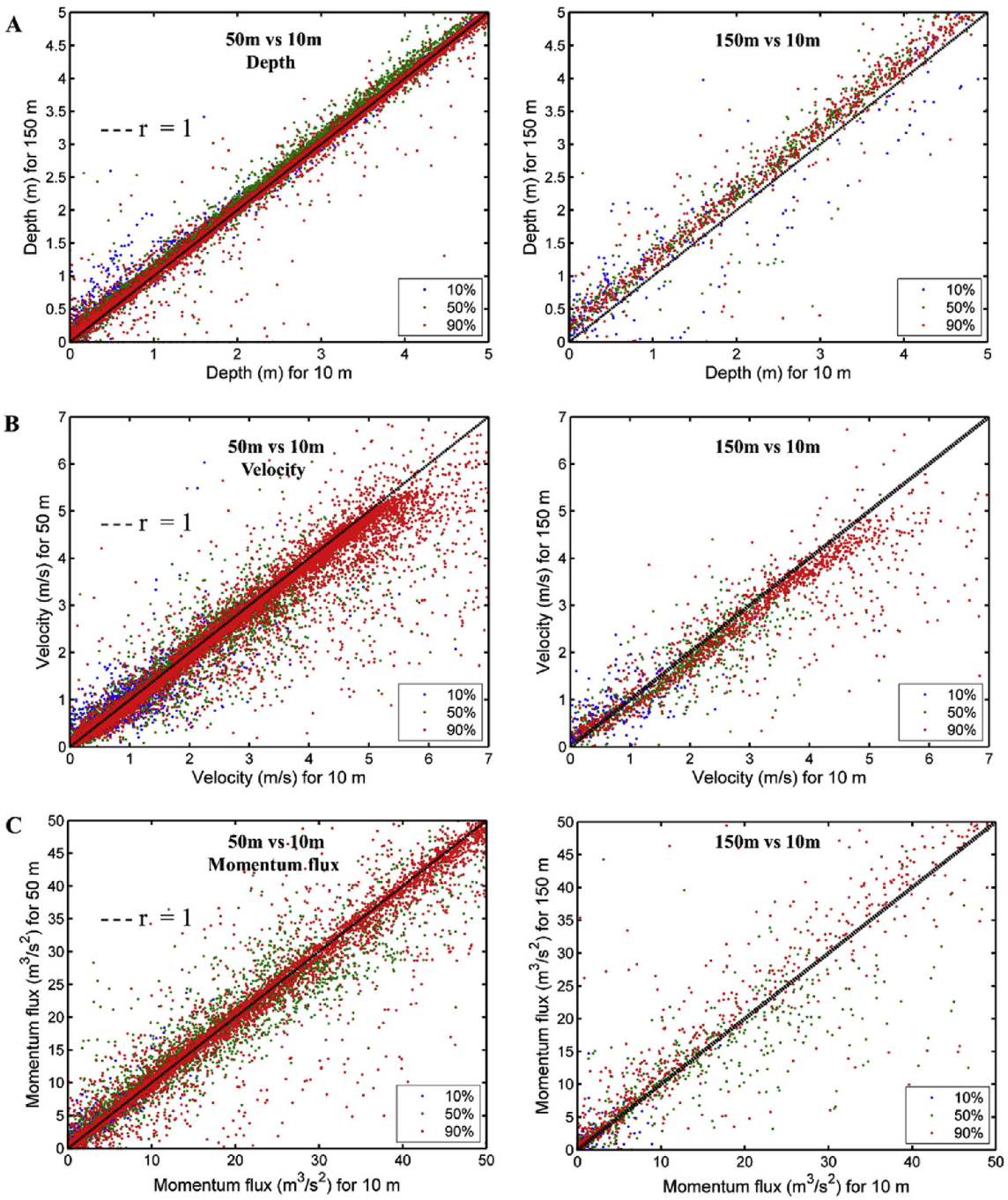

Fig. 13. Tsunami hazard parameter comparison for stochastic models. (A) Depth. (B) Velocity. (C). Momentum flux. (r = correlation coefficient).

50-m grids are similar, whilst for the 150-m grid, the depth maps for all three percentile ranks are slightly different compared to the other two specifically near the ocean and rivers (see Fig. 7). Moreover, the inundation areas indicated in Fig. 7 quantify the tsunami depth differences due to the use of three different DEM resolutions. In general, the higher elevation resolution results in larger inundation areas. However, the differences of inundation areas from the three grids are considered being small, i.e. the percentage differences of the inundation from the 50-m grid and the 150-m grid against the 10-m grid are only ~5%.

To investigate the differences of tsunami depth, more local areas of Padang, i.e. Teluk Bayur (see the red rectangle in the left panel of Fig. 7A), are focused upon. Fig. 8 shows that the depth maps for the 10-m and 50-m grids are similar. Nevertheless, the 50-m resolution may not capture detailed spatial features of the tsunami hazard along the coastal line (see white rectangle areas in Fig. 8A and B). In addition, the 150-m grid results are not accurate along the coast. Several significant tsunami depth areas found in the 10-m and the 50-m grids disappear in the 150-m grid cases.

On the other hand, the maximum tsunami velocity in Padang is about 7 m/s which is mainly found in the areas near the coast and rivers (see Figs. 9 and 10). In general, the tsunami wave velocity is higher at finer elevation resolution (i.e. 10 m). Moreover, the 150-m grid may not capture accurate tsunami velocity profiles specifically near the coast. Finally, the momentum flux comparisons are presented in Figs. 11 and 12. The figures show that the 50-m and the 150-m grids may underestimate the momentum flux. The 90th percentile rank event of the 10-m

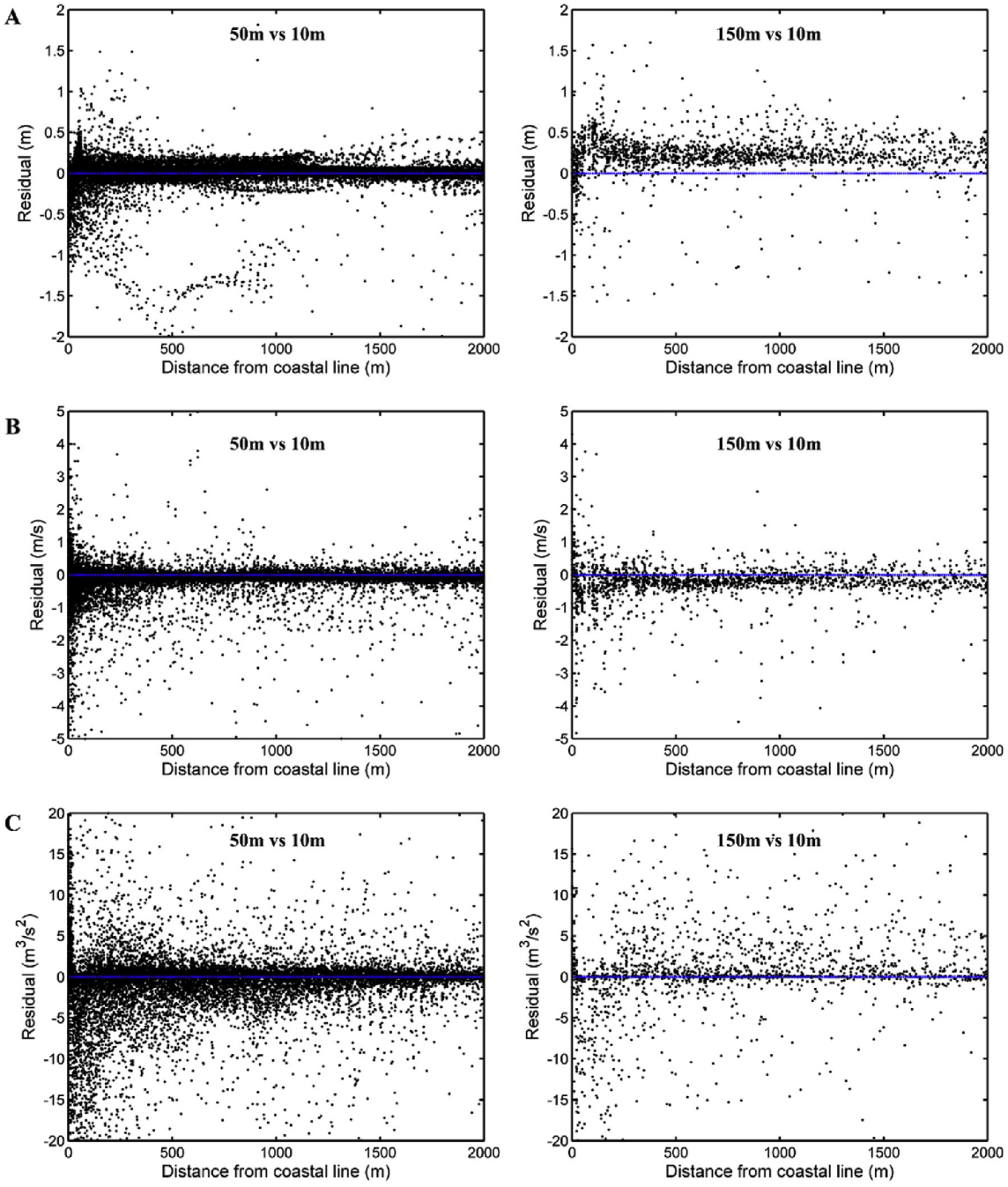

Fig. 14. Residual of grid comparisons for stochastic models. (A) Depth. (B) Velocity. (C). Momentum flux.

grids is almost covered by red color (~250 m^3/s^2). In contrast, the 50-m and the 150-m grids visualize relatively smaller momentum flux, e.g. several parts are in yellow color.

In addition, Fig. 13 and Fig. 14 show the comparisons of the three tsunami hazard parameters of two grids (coarser grid versus finer grid) and their residual plots against the distance from the coastal line, respectively. The residual is calculated by taking the difference between the larger grid and the smaller grid. A diagonal dashed-black line in Fig. 13 corresponds to the perfect positive correlation coefficient, *r*, equal to 1, whilst the blue line in Fig. 14 represents a zero-difference base line. In general, the figures show that most of the depth data for the 50-m and 10-m grids are almost identical, whilst the 150-m resolution results are typically overestimated in comparison to the base case (i.e. the 10-m grid). However, the differences are mostly minor, i.e. less than 0.5 m. On the other hand, the velocity comparison confirms that a larger grid (i.e. the 50-m and the 150-m grids) underestimates flow velocity in comparison to a finer grid (i.e. 10-m grid). In addition, the variability of velocity differences between the 10-m and the other grids is larger than the tsunami depth parameter. The results also exhibit that momentum flux is the most sensitive to the DEM resolutions among the three hazard parameters. The main reason is because the momentum flux calculation incorporates both depth and velocity parameters (see Equation (3)) that can significantly increase the variability of momentum flux differences. Another important finding is that the three tsunami hazard parameters are sensitive to the DEM resolution when it is located closer to coastal line (<1 km).

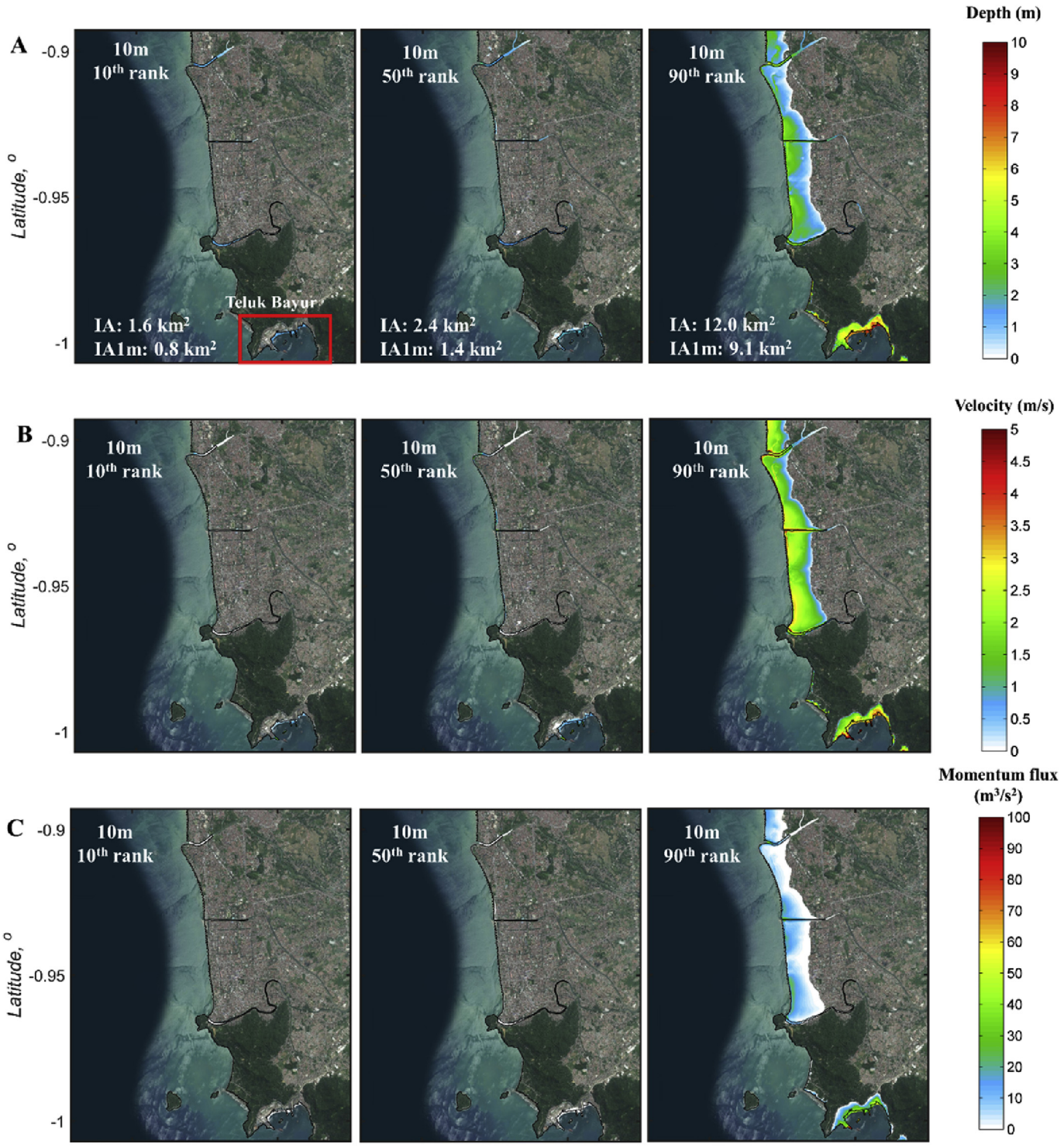

Fig. 15. Tsunami hazard maps in Padang from uniform models of 10-m grid. (A) Depth. (B) Velocity. (C). Momentum flux. (IA = Inundation area; IA1m = Inundation area above 1 m depth).

3.2. Effect of earthquake source model complexity on tsunami hazard assessment

To examine the effect of earthquake source model complexity on tsunami hazard assessment, tsunami hazard map profiles in terms of depth, flow velocity, and momentum flux produced from the 10-m DEM using uniform models are presented in Fig. 15 and Fig. 16 for Padang and Teluk Bayur, respectively. The counterparts of the stochastic source models are shown in Figs. 7A, 9A and 11A for Padang and Figs. 8A, 10A and 12A for Teluk Bayur. The map comparisons in Fig. 7 versus Fig. 15A clearly indicate that the inundation areas predicted in the uniform models is two to three times smaller than the inundation areas calculated in the stochastic models. The residuals calculated by taking the difference between the uniform models over the stochastic models for all percentiles shown in Fig. 17A also confirm that the uniform model majorly underestimates the depth in comparison to the stochastic models.

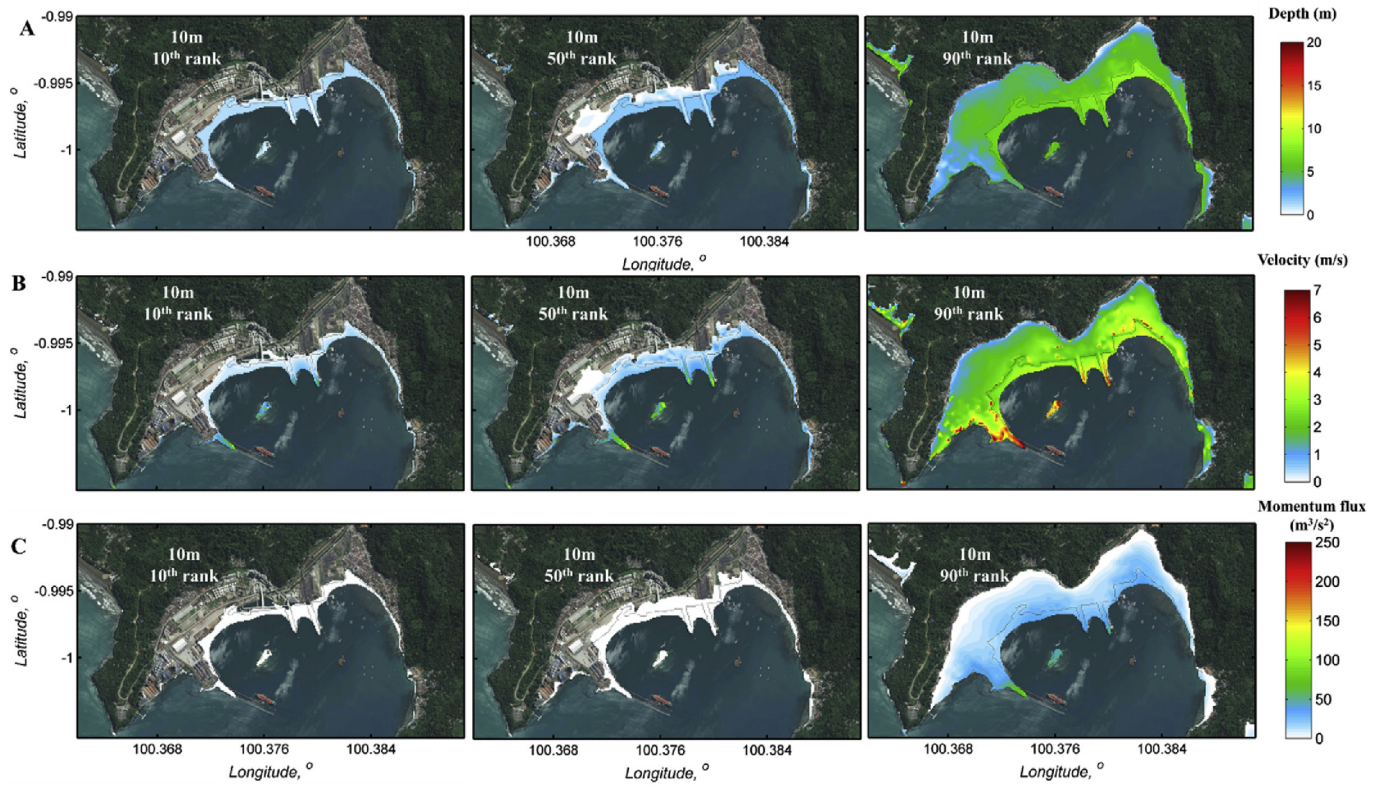

Fig. 16. Tsunami hazard maps in Teluk Bayur from uniform models of 10-m grid. (A) Depth. (B) Velocity. (C). Momentum flux.

For flow velocity and momentum flux, the uniform models also substantially underestimate the hazard parameters. As presented in the zoom red rectangle areas in Teluk Bayur for both parameters (see Fig. 16B and C), the results from the uniform models predict much smaller velocity and momentum flux in comparison to the stochastic models (Figs. 10A and 12A). Flow velocities at all probability ranks in Fig. 17 are majorly overestimated specifically for larger velocity values. The differences in terms of residual for velocity also corroborate this trend. The differences reach up to 10 m/s. For momentum flux, the differences even become greater (up to 4 times differences) since it is calculated by considering both tsunami depth and velocity parameters.

In general, the above-mentioned results indicate that the tsunami hazard parameters, i.e. depth, velocity, and momentum flux, are more sensitive to the earthquake slip models than the grid resolution. Note that the differences between the complex and uniform models are attributed to earthquake slip heterogeneity only (other earthquake source parameters, e.g. geometry and mean slip, are identical). Substantial underestimation of tsunami depth/height may produce inaccurate tsunami hazard maps that are currently in use for developing tsunami evacuation plans. Subsequently, the consequences due the use of uniform models to develop tsunami evacuation plans may be significant. On the other hand, flow velocity and momentum flux are also essential to determine the building damage state and hence, by using the uniform models, tsunami risk assessments may be inaccurate. Accordingly, mitigation policies producing from such analyses may also be unreliable and may not be implemented effectively in coastal community.

3.3. *Effect of DEM resolution and earthquake source model complexity on fatality estimation*

Using tsunami height and depth parameters calculated from all cases, the fatality is further estimated (see the ***Fatality estimation*** section). To calculate the fatality, all tsunami height/depths produced from different DEM resolutions are linearly interpolated at the grid points of WorldPop. Using Equation (4), the total fatality is then calculated by considering the death rate based on the four fatality models (Fig. 6).

Generally, the fatality estimation clearly shows the importance of reducing the fatality in coastal areas because the estimated fatality numbers are generally high. Existing of tsunami evacuation plan in coastal areas is also essential to reduce the fatality number. As shown in Table 3, for the worst scenario (the 90th probability rank), the fatality could be reduced significantly (up to ~97%) when the people are effectively evacuated. Although the fatality models used in this study may involve large uncertainties in calculating the fatality (e.g. only considering one tsunami hazard parameter), it clearly highlights that tsunami evacuation drills are essential to be carried out in coastal community. By increasing the awareness of tsunami evacuation plan in a tsunami-prone region, the fatality could be reduced substantially. Moreover, Table 3 also underlines huge human loss due to the future megathrust earthquake from the Mentawai segment in Padang areas. The fatality could be as much as 200,000 people as estimated using model 1 which is almost 75% of the total population of Padang in coastal areas. Emergency managers in Padang should be aware of potentially devastating tsunami losses and strive to reduce the human losses in the near future due to the tsunamigenic events.

Regarding the DEM resolution effects on fatality estimation, Table 4 presents the percentage difference between the finer grid and the coarser grid (i.e. the 10-m grid vs the 50-m grid and the 10-m grid vs the 150-m grid). Negative percentage in the table means that the finer grid underestimates the fatality in comparison to the coarser grid. In general, all comparisons confirm only ~5% differences in terms of fatality specifically for the 50th and 90th percentile ranks. However, the coarser grid seems to underestimate the fatality for the 10th percentile rank. It is mainly due to significant values of depths above 1 m that are underestimated for the coarser grid in the 10th percentile rank compared to the finer grid (see Fig. 13). The fatality differences tend to be substantial

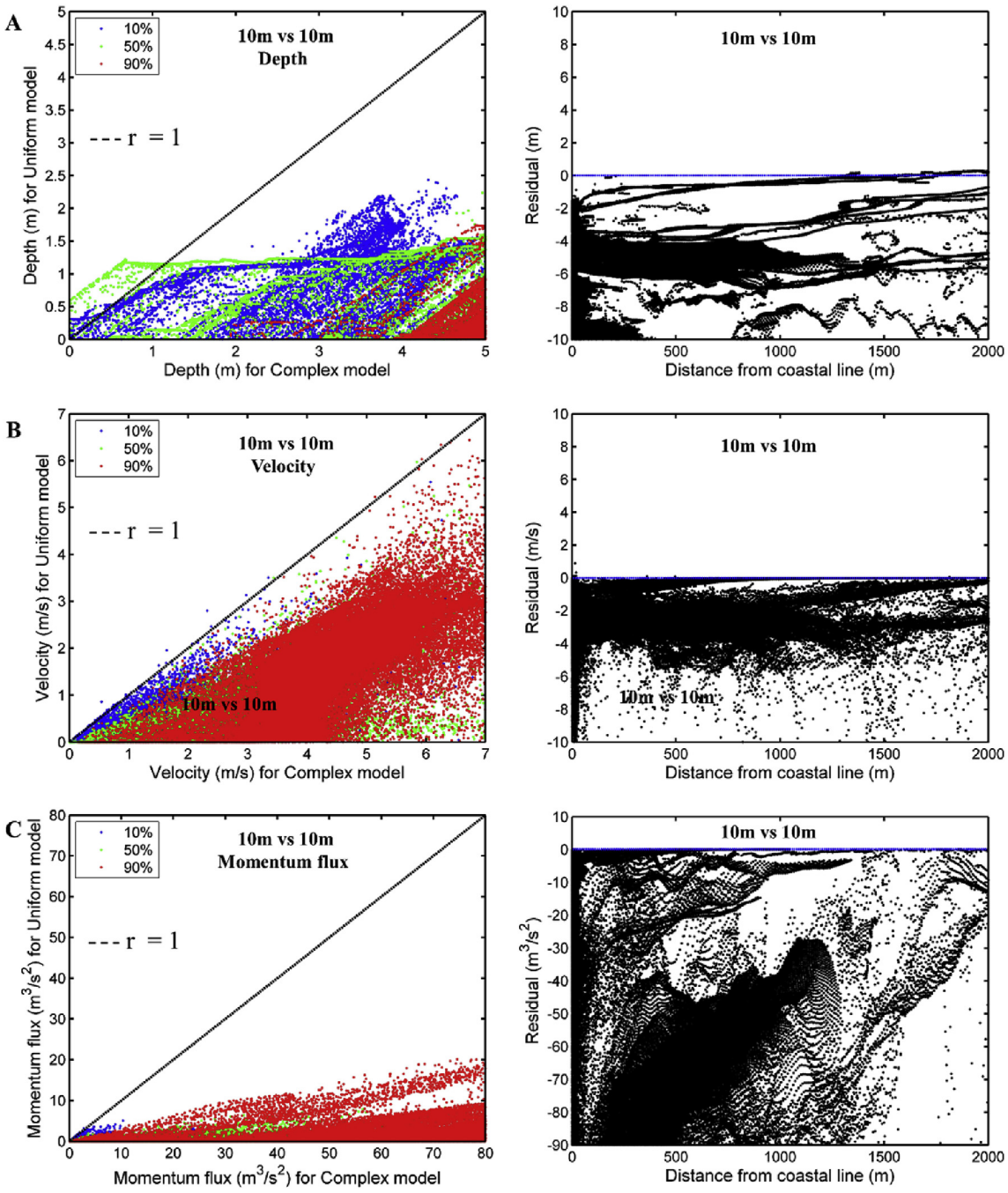

Fig. 17. Depth comparison between stochastic and uniform models for 10-m grid. (A) Depth. (B) Velocity. (C). Momentum flux. (r = correlation coefficient).

when the comparison is carried out between the complex and the uniform models, i.e. it ranges from 78% to 100% (see Table 4).

The results on fatality estimation confirm that the complexity of earthquake source characterization significantly influences the fatality number estimation. Subsequently, realistic tsunamigenic earthquake source models (i.e. stochastic models) generated by taking into account all uncertainty of earthquake source parameters, are essential to produce accurate and reliable tsunami risk estimation. Lack of earthquake source modeling, in particular slip heterogeneity modeling, may lead to inaccurate prediction of human losses. Such inaccurate prediction may further influence on the development of tsunami mitigation policies in coastal community. For instance, tsunami evacuation shelters may not be built in high risk human losses areas due to underestimating the fatality number in that region. Thus, major undesirable consequences might be caused from inaccurate earthquake source modeling.

3.4. Recommendations for tsunami disaster risk management

Extensive tsunami hazard assessments by considering different DEM resolution and source model complexity may suggest several essential recommendations for tsunami disaster risk management purposes. Firstly, accurate earthquake slip modeling is essential to produce reliable tsunami hazard and risk assessments. In this study, the earthquake slip is found to be a major source of uncertainty affecting the tsunami simulation results significantly and hence, the implementation of stochastic earthquake source modeling is deemed essential to develop rigorous and

Table 3
Estimated fatality (in people) from all cases.

Stochastic model												
Grid resolution	10-m				50-m				150-m			
Casualty model	Model 1	Model 2	Model 3	Model 4	Model 1	Model 2	Model 3	Model 4	Model 1	Model 2	Model 3	Model 4
10th percentile	3007	0	1234	405	2878	0	1177	385	2759	0	1140	272
50th percentile	71093	180	31821	5090	71547	177	32002	5007	69971	179	31303	4542
90th percentile	201384	2702	103471	19999	196465	2639	99779	19252	189500	2678	96307	18481
Uniform model												
Grid resolution	10-m				50-m				150-m			
Casualty model	Model 1	Model 2	Model 3	Model 4	Model 1	Model 2	Model 3	Model 4	Model 1	Model 2	Model 3	Model 4
10th percentile	1	0	0	66	0	0	0	7	0	0	0	0
50th percentile	48	0	15	151	20	0	6	18	0	0	0	1
90th percentile	44354	56	19693	3020	43098	44	19116	2944	42682	45	18942	2699

Table 4
Comparison of estimated fatality.

Effect of DEM resolution								
Grid resolution	10 m vs 50 m				10 m vs 150 m			
Fatality model	Model 1 (%)	Model 2 (%)	Model 3 (%)	Model 4 (%)	Model 1 (%)	Model 2 (%)	Model 3 (%)	Model 4 (%)
10th percentile	4	0	5	5	8	0	8	33
50th percentile	−1	2	−1	2	2	1	2	11
90th percentile	2	2	4	4	6	1	7	8
Effect of earthquake source model complexity								
Grid resolution	10 m vs 10 m				50 m vs 50 m			
Fatality model	Model 1 (%)	Model 2 (%)	Model 3 (%)	Model 4 (%)	Model 1 (%)	Model 2 (%)	Model 3 (%)	Model 4 (%)
10th percentile	100	0	100	84	100	0	100	98
50th percentile	100	100	100	97	100	100	100	100
90th percentile	78	98	81	85	78	98	81	85

robust tsunami hazard assessment and fatality estimation in a region of interest. Secondly, at least a 10-m or 50-m grid is recommended for tsunami hazard assessment purposes using depth parameter. However, detailed tsunami depth assessment along coastal lines should be carried out using the 10-m or finer resolution. Thirdly, when the flow velocity and momentum flux are taken into account, finer grids (<10-m) are needed specifically within the range of 1 km from the coastal line.

Finally, the extensive tsunami hazard and risk analyses carried out in this study, demonstrate the possibility of creating new big data information for tsunami disaster risk management purposes. The tsunami hazard potential may be presented rigorously for different probability ranks (represented by a set of tsunami hazard maps, in sharp contrast with conventional single worst-case hazard map) and further explored to create big data information of tsunami hazard level in a region of interest. Such information is valuable for the emergency managers to develop effective tsunami mitigation policies in coastal community. Rigorous information of tsunami hazard parameters from wave height and depth to flow velocity and momentum flux in a region of interest may also be generated through extensive tsunami simulations specifically by incorporating stochastic earthquake source scenarios. Those hazard parameters are important to calculate the tsunami risk in terms of economic and human losses, as demonstrated in the case study of this work. This will allow the related managers to give strong recommendations for the local authorities to implement risk management strategies in coastal community.

4. Conclusions

The main purpose of this study was to examine the effects of DEM resolutions and complexity of earthquake source characterization on tsunami hazard assessment and fatality estimation. To investigate such purpose, three DEM resolutions including the 10-m, the 50-m, and the 150-m grids were adopted using two different earthquake source models, i.e. the stochastic and the uniform source models. Both the stochastic and uniform models had identical geometry but varying in slip value. The stochastic earthquake source models incorporated heterogeneity of spatial earthquake slip parameter, whilst the uniform models only used mean slip as the only to represent earthquake slip over the fault-plane. Subsequently, the tsunami hazard assessments in terms of depth, velocity and momentum fluxes in Padang areas were assessed by considering both different DEM grid resolutions and earthquake source model complexity. The tsunami hazard maps for the three parameters were developed for three probability ranks, i.e. the 10th, the 50th and the 90th percentile ranks, and were used to evaluate the differences in terms of tsunami hazard potential. Finally, the fatality was estimated to study the effect of DEM resolutions and earthquake source model complexity on fatality estimation.

The results show that the tsunami depth is less sensitive to the DEM resolutions in comparison to the flow velocity and momentum flux. However, all hazard parameters are more sensitive to the earthquake slip models than the grid resolutions. The tsunami hazard parameters are significantly underestimated in the uniform models compared to the stochastic models. The fatality estimation is also found to be more sensitive to the earthquake source models, in particular, earthquake slip, than the grid resolution. This highlights that accurate and reliable tsunamigenic earthquake source models (e.g. stochastic models) generated by taking into account all uncertainty and dependency of earthquake source parameters are essential to produce tsunami risk estimation. Moreover, the results also show that the 10-m grid developed from extensive geosciences measurements is extremely useful to improve the quality assessment of tsunami hazard. The availability of such datasets improves the tsunami preparedness by providing rigorous and extensive

information of tsunami hazard maps using various parameters from depth, velocity to momentum flux and hence, is essentially needed for developing reliable mitigation strategies.

Lastly, although the tsunami hazard assessment and fatality estimation in Padang were carried out using the results of rigorous stochastic tsunami simulations, there are limitations that need to be addressed in future studies. These include: (1) taking into account the building information data for tsunami inundation modeling to capture the tsunami hazard inland more realistically, (2) incorporating earthquake impacts on the fatality estimation, and (3) other impact metrics, such as building damage and loss, should be taken into account when assessing the earthquake risk in Padang.

Acknowledgments

The first author is grateful to the Directorate General of Resources for Science, Technology and Higher Education, Ministry of Research, Technology and Higher Education of Indonesia for sponsoring his PhD study. This work is also funded by the Engineering and Physical Sciences Research Council (EP/M001067/1). The authors are grateful to Widjo Kongko who provides DEM and bathymetry data for Padang. The bathymetry and elevation data for the Sumatra region were obtained from the GEBCO2014 database (http://www.gebco.net/data_and_products/gridded_bathymetry_data/) and the GDEM2 database (https://asterweb.jpl.nasa.gov/gdem.asp), respectively.

References

Abril, J.M., Periáñez, R., 2017. A modelling study on tsunami propagation in the Red Sea: historical events, potential hazards and spectral analysis. Ocean Eng. 134 (2017), 1–12. ISSN 0029-8018. https://doi.org/10.1016/j.oceaneng.2017.02.008.

Alvina, K., Kuncoro, Cubas, N., Singh, S.C., Etchebes, M., Tapponnier, P., 2015. Tsunamigenic potential due to frontal rupturing in the Sumatra locked zone. Earth Planet Sci. Lett. 432 (2015), 311–322. ISSN 0012-821X. https://doi.org/10.1016/j.epsl.2015.10.007.

Attary, N., Unnikrishnan, V.U., van de Lindt, J.W., Cox, D.T., Barbosa, A.R., 2017. Performance-Based Tsunami Engineering methodology for risk assessment of structures. Eng. Struct. 141 (2017), 676–686. ISSN 0141-0296. https://doi.org/10.1016/j.engstruct.2017.03.071.

Badan Pusat Statistik (BPS) Kota Padang, 2013. Data Penduduk Kota Padang Tahun 2013. Badan Pusat Statistik, Padang, Indonesia.

Charvet, I., Suppasri, A.H., Kimura, D., Sugawara, F., Imamura, A., 2015. Multivariate Generalized Linear Tsunami Fragility Model for Kesennuma City Based on Maximum Flow Depths, Velocities and Debris Impact, with Evaluation of Predictive Accuracy, Natural Hazards, pp. 1–27. https://doi.org/10.1007/s11069-015-1947-8.

Chorafas, D.N., 2004. 10-The science of insurance and the notion of technical risk. In: Operational Risk Control with Basel II, Butterworth-heinemann, Oxford, vol. 2004, pp. 209–229. ISBN 9780750659093. https://doi.org/10.1016/B978-075065909-3.50012-8.

De Risi, R., Goda, K., 2016. Probabilistic earthquake–tsunami multi-hazard analysis: application to the Tohoku region, Japan. Frontiers Built Environment 2, 25. https://doi.org/10.3389/fbuil.2016.00025.

De Risi, R., Goda, K., Yasuda, T., Mori, N., 2017. Is flow velocity important in tsunami empirical fragility modeling?, 2017. Earth Sci. Rev. 166, 64–82. ISSN 0012-8252. https://doi.org/10.1016/j.earscirev.2016.12.015.

Diana, J.M., Greenslade, Annunziato, A., Babeyko, A.Y., Burbidge, D.R., Ellguth, E., Horspool, N., Kumar, T.S., Kumar, C.P., Moore, C.W., Rakowsky, N., Riedlinger, T., Ruangrassamee, A., Srivihok, P., Titov, V.V., 2014. An assessment of the diversity in scenario-based tsunami forecasts for the Indian Ocean. Continent. Shelf Res. 79, 36–45. ISSN 0278-4343. https://doi.org/10.1016/j.csr.2013.06.001.

Farahani, R.J., Woessner, J., Bingi, S., Charvet, I., Williams, Ch, Nyst, M., Masuda, M., Bryngelson, J., Shome, N., 2017. Tsunami risk for insurance portfolios from megathrust earthquakes in Cascadia subduction zone. In: Paper presented at the 16th World Conference on Earthquake Engineering, Santiago de Chile.

FEMA (Federal Emergency Management Agency), 2012. P-646: Guidelines for Design of Structures for Vertical Evacuation from Tsunamis, second ed. Federal Emergency Management Agency, Washington, D.C.

Feng, X., Yin, B., Gao, S., Wang, P., Bai, T., Yang, D., 2017. Assessment of tsunami hazard for coastal areas of Shandong Province, China. Appl. Ocean Res. 62 (2017), 37–48. ISSN 0141-1187. https://doi.org/10.1016/j.apor.2016.12.001.

Goda, K., Mai, P.M., Yasuda, T., Mori, N., 2014. Sensitivity of tsunami wave profiles and inundation simulations to earthquake slip and fault geometry for the 2011 Tohoku earthquake. Earth Planets Space 66, 105. https://doi.org/10.1186/1880-5981-66-105.

Goda, K., Yasuda, T., Mori, N., Maruyama, T., 2016. New scaling relationships of earthquake source parameters for stochastic tsunami simulation. Coast Eng. J. https://doi.org/10.1142/S0578563416500108.

Goto, C., Ogawa, Y., Shuto, N., Imamura, F., 1997. Numerical Method of Tsunami Simulation with the Leap-frog Scheme. IOC Manual, vol. 35. UNESCO, Paris, France.

Griffin, J., Latief, H., Kongko, W., Harig, S., Horspool, N., Hanung, R., Rojali, A., Maher, N., Fuchs, A., Hossen, J., Upi, S., Dewanto, E., Rakowsky, N., Cummins, P., 2015. An evaluation of onshore digital elevation models for modeling tsunami inundation zones. Front. Earth Sci. 3 (32) https://doi.org/10.3389/feart.2015.00032.

Iida, K., 1959. Earthquake energy and earthquake fault, Nagoya University. Journal of Earth Science 7, 98–107.

Imamura, F., 2009. Tsunami modelling: calculating inundation and hazard maps. In: Bernard, E., Robinson, A. (Eds.), Tsunamis. The Sea, Ideas and Observations on Progress in the Studies of the Sea, vol. 15. Harvard University Press, Cambridge, MA, pp. 321–332.

Ismail-Zadeh, A., Soloviev, A., Vladimir Sokolov, V., Inessa Vorobieva, I., Müller, B., Schilling, F., 2017. Quantitative Modeling of the Lithosphere Dynamics, Earthquakes and Seismic Hazard, Tectonophysics. Available online 8 April 2017, ISSN 0040-1951. https://doi.org/10.1016/j.tecto.2017.04.007.

Kaiser, G., Scheele, L., Kortenhaus, A., Løvholt, F., Romer, H., Leschka, 2011. The influence of land cover roughness on the results of high resolution tsunami inundation modeling. Nat. Hazards Earth Syst. Sci. 11, 2521–2540.

Kawata, Y., 1997. Prediction of loss of human lives due to catastrophic earthquake disaster. Japan society for natural disaster science 16 (1), 3–13 (In Japanese).

King, D.N., 2015. Tsunami hazard, assessment and risk in Aotearoa–New Zealand: a systematic review AD 1868–2012. Earth Sci. Rev. 145 (2015), 25–42. ISSN 0012-8252. https://doi.org/10.1016/j.earscirev.2015.02.004.

Mai, P.M., Beroza, G.C., 2002. A spatial random field model to characterize complexity in earthquake slip. J. Geophys. Res.: Solid Earth 107. https://doi.org/10.1029/2001JB000588.

Mai, P.M., Thingbaijam, K.K.S., 2014. SRCMOD: an online database of finite-fault rupture models. Seismol Res. Lett. 85, 1348–1357.

Marchand, M., Buurman, J., Pribadi, A., Kurniawan, A., 2009. Damage and casualties modelling as part of a vulnerability assessment for tsunami hazards: a case study from Aceh, Indonesia. Journal of Flood Risk Management 2, 120–131. https://doi.org/10.1111/j.1753-318X.2009.01027.x.

Martínez-Álvarez, F., Gutiérrez-Avilés, Morales-Esteban, A., Reyes, J., Amaro-Mellado, J.L., Rubio-Escudero, C., 2015. A novel method for seismogenic zoning based on triclustering: application to the Iberian Peninsula. Entropy 17, 5000–5021. https://doi.org/10.3390/e17075000.

Mori, N., Muhammad, A., Goda, K., Yasuda, T., Ruiz-Angulo, A., 2017. Probabilistic tsunami hazard analysis of the Pacific coast of Mexico: case study based on the 1995 colima earthquake tsunami. Front. Built Environ 3, 34. https://doi.org/10.3389/fbuil.2017.00034.

Mueller, C., Power, W., Fraser, S., Wang, X., 2015. Effects of rupture complexity on local tsunami inundation: implications for probabilistic tsunami hazard assessment by example. Journal Geophysical Research Solid Earth 120, 488–502. https://doi.org/10.1002/2014JB011301.

Muhammad, A., Goda, K., Alexander, N., 2016. Tsunami hazard analysis of future megathrust sumatra earthquakes in padang, Indonesia using stochastic tsunami simulation. Frontiers Built Environment 2 (33). https://doi.org/10.3389/fbuil.2016.00033.

Muhammad, A., Goda, K., Alexander, N.A., Kongko, W., Muhari, A., 2017. Tsunami evacuation plans for future megathrust earthquakes in Padang, Indonesia, considering stochastic earthquake scenarios. Nat. Hazards Earth Syst. Sci. 17, 2245–2270. https://doi.org/10.5194/nhess-2017-75.

Muhari, A., Imamura, F., Natawidjaja, D.H., Diposaptono, S., Latief, H., Post, J., et al., 2010. Tsunami mitigation efforts with pTA in West sumatra Province, Indonesia. Journal of Earthquake and Tsunami 4, 341–368. https://doi.org/10.1142/S1793431110000790.

Muhari, A., Imamura, F., Koshimura, S., Post, J., 2011. Examination of three practical run-up models for assessing tsunami impact on highly populated areas. Nat. Hazards Earth Syst. Sci. 11, 3107–3123. https://doi.org/10.5194/nhess-11-3107-2011.

Mulyani, R., 2013. Extended framework for earthquake and tsunami risk assessment: padang city a case study. In: Civil and Structural Engineering. The University of Sheffield, Sheffield, UK.

Murotani, S., Satake, K., Fujii, Y., 2013. Scaling relations of seismic moment, rupture area, average slip, and asperity size for M9 subduction-zone earthquakes. Geophys. Res. Lett. 40, 5070–5074.

Okada, Y., 1985. Surface deformation due to shear and tensile faults in a half-space. Bull. Seismol. Soc. Am. 75, 1135–1154.

Park, H., Cox, D.T., 2016. Probabilistic assessment of near-field tsunami hazards: inundation depth, velocity, momentum flux, arrival time, and duration applied to Seaside, Oregon. Coast Eng. 117 (2016), 79–96. ISSN 0378-3839. https://doi.org/10.1016/j.coastaleng.2016.07.011.

Park, H., Cox, D.T., Barbosa, A.R., 2017. Comparison of inundation depth and momentum flux based fragilities for probabilistic tsunami damage assessment and uncertainty analysis. Coast Eng. 122 (2017), 10–26. ISSN 0378-3839. https://doi.org/10.1016/j.coastaleng.2017.01.008.

Ramírez-Juidías, E., Víquez-Urraco, F., Noguero-Hernández, D., 2017. Sedimentary processes in the Isla Cristina salt-marshes: geomorphological changes of landscape. Ocean Coast Manag. 143, 148–153. https://doi.org/10.1016/j.ocecoaman.2016.11.007.

Ridente, D., Martorelli, E., Bosman, A., Chiocci, F.L., 2014. 2014. High-resolution morpho-bathymetric imaging of the Messina Strait (Southern Italy). New insights on the 1908 earthquake and tsunami. Geomorphology 208, 149–159. ISSN 0169-555X. https://doi.org/10.1016/j.geomorph.2013.11.021.

Schäfer, A.M., Wenzel, F., 2017. TsuPy: computational robustness in Tsunami hazard modelling. Comput. Geosci. 102 (2017), 148–157. ISSN 0098-3004. https://doi.org/10.1016/j.cageo.2017.02.016.

Schlurmann, T., Kongko, W., Goseberg, N., Natawidjaja, D.H., Sieh, K., 2010. Near-field tsunami hazard map padang, west sumatra: utilizing high resolution geospatial data and reasonable source scenarios. Coastal Engineering Proceeding 32, 1–17. https://doi.org/10.9753/icce.v32.management.26.

Sleeter, B.M., Wood, N.J., Soulard, C.E., Wilson, T.S., 2017. 2017. Projecting community changes in hazard exposure to support long-term risk reduction: a case study of tsunami hazards in the U.S. Pacific Northwest. International Journal of Disaster Risk Reduction 22, 10–22. ISSN 2212-4209. https://doi.org/10.1016/j.ijdrr.2017.02.015.

Somerville, P., Irikura, K., Graves, R., Sawada, S., Wald, D., Abrahamson, N., Iwasaki, Y., Kagawa, T., Smith, N., Kowada, A., 1999. Characterizing crustal earthquake slip models for the prediction of strong ground motion. Seismol Res. Lett. 70, 59–80.

Srisutam, C., Wagner, J., 2010. Reconstructing tsunami run-up from the characteristics of tsunami deposits on the Thai Andaman Coast. Coast Eng. 57 (5), 493–499. ISSN 0378-3839. https://doi.org/10.1016/j.coastaleng.2009.12.001.

Strasser, F., Arango, M., Bommer, J.J., 2010. Scaling of the source dimensions of interface and intraslab subduction-zone earthquakes with moment magnitude. Seismol Res. Lett. 81, 941–950.

Sugawara, D., Goto, K., 2012. Numerical modeling of the 2011 Tohoku-oki tsunami in the offshore and onshore of Sendai Plain, Japan. Sediment. Geol. 282, 110–123. https://doi.org/10.1016/j.sedgeo.2012.08.002.

Suppasri, A., Imamura, F., Koshimura, S., 2012. Tsunami hazard and casualty estimation in a coastal area that neighbors the Indian Ocean and South China Sea. Journal of Earthquake and Tsunami 6, 1250010. https://doi.org/10.1142/S1793431112500108.

Suppasri, A., Hasegawa, N., Makinoshima, F., Imamura, F., Latcharote, P., Day, S., 2016. An analysis of fatality ratios and the factors that affected human fatalities in the 2011 great East Japan tsunami. Frontiers Built Environment 2 (32). https://doi.org/10.3389/fbuil.2016.00032.

Tanioka, Y., Satake, K., 1996. Tsunami generation by horizontal displacement of ocean bottom. Geophys. Res. Lett. 23, 861–864.

Taubenbock, H., Goseberg, N., Setiadi, N., Lammel, G., Moder, F., Oczipka, M., Klupfel, H., Wahl, R., Schlurmann, T., Strunz1, G., Birkmann, J., Nagel, K., Siegert, K., Lehmann, F., Dech, S., Gress, A., Klein, R., 2009. "Last-Mile" preparation for a potential disaster – interdisciplinary approach towards tsunami early warning and an evacuation information system for the coastal city of Padang, Indonesia. Nat. Hazards Earth Syst. Sci. 9, 1509–1528. https://doi.org/10.5194/nhess-9-1509-2009.

Thingbaijam, K.K.S., Martin Mai, P., Goda, K., 2017. New empirical earthquake source-scaling laws. Bull. Seismol. Soc. Am. 107 (5), 2225–2246.

Tocher, D., 1958. Earthquake energy and ground breakage. Bull. Seismol. Soc. Am. 48, 147–153.

Wang, C., Ding, X., Li, Q., Shan, X., Zhu, W., Guo, B., Liu, P., 2015. Coseismic and postseismic slip models of the 2011 Van earthquake, Turkey, from InSAR, offset-tracking, MAI, and GPS observations. J. Geodyn. 91 (2015), 39–50. ISSN 0264-3707. https://doi.org/10.1016/j.jog.2015.08.006.

Wells, D.L., Coppersmith, K.J., 1994. New empirical relationships among magnitude, rupture length, rupture width, rupture area, and surface displacement. Bull. Seismol. Soc. Am. 84, 974–1002.

Wilkinson, S.M., Alarcon, J.E., Mulyani, R., Whittle, J., Chian, S.C., 2012. Observations of damage to buildings from mw 7.6 padang earthquake of 30 September 2009. Nat. Hazards 63 (2), 521–547.

Yeh, H., 2010. Gender and age factor on tsunami casualties. Nat. Hazards Rev. 11, 29–34. https://doi.org/10.1061/(ASCE)1527-6988(2010)11:1(29).

Yue, H., Lay, T., Rivera, L., Bai, Y., Yamazaki, Y., Cheung, K.F., et al., 2014. Rupture process of the 2010 Mw7.8 Mentawai tsunami earthquake from joint inversion of near-field hr-GPS and teleseismic body wave recordings constrained by tsunami observations. J. Geophys. Res. Solid Earth 119, 5574–5593. https://doi.org/10.1002/2014JB011082.